Manuscript prepared for Clim. Past Discuss.
with version 2014/05/30 6.91 Copernicus papers of the LaTeX class copernicus.cls.
Date: 12 January 2015

Implementation of counted layers for coherent ice core chronology

B. Lemieux-Dudon[1], L. Bazin[2], A. Landais[2], M. Guillevic[2,3], P. Kindler[4], F. Parrenin[5], and P. Martinerie[5]

[1]Laboratoire Jean Kuntzmann, Grenoble, France
[2]Laboratoire des Sciences du Climat et de l'Environnement, UMR8212, CEA–CNRS–UVSQ, Orme des Merisiers, Gif sur Yvette, France
[3]Centre for Ice and Climate, Niels Bohr Institute, University of Copenhagen, Copenhagen, Denmark
[4]Climate and Environmental Physics, Physics Institute & Oeschger Center for Climate Change Research, University of Bern, Bern, Switzerland
[5]Laboratoire de Glaciologie et Géophysique de l'Environnement, UMR 5183, Univ. Grenoble Alpes–CNRS, Grenoble, France

Correspondence to: Lucie Bazin, lucie.bazin@lsce.ipsl.fr

Abstract

A recent coherent chronology has been built for 4 Antarctic ice cores and the NorthGRIP (NGRIP) Greenland ice core (Antarctic Ice Core Chronology 2012, AICC2012) using a bayesian approach for ice core dating (Datice). When building the AICC2012 chronology, and in order to prevent any confusion with official ice cores chronology, the AICC2012 chronology for NGRIP was forced to fit exactly the GICC05 chronology based on layer counting. However, such a strong tuning did not satisfy the hypothesis of independence of background parameters and observations for the NGRIP core, as required by Datice. We present here the implementation in Datice of a new type of markers that is better suited for constraints deduced from layer counting: the markers of age–difference. Estimating the global error on chronology from such markers is not straightforward and implies some assumption on the correlation between individual counting errors for each interval of age difference. We validate this new methodological implementation by conducting twin experiments on the NGRIP ice core and performing several sensitivity tests on sampling and correlation between counting errors to come up with some guidelines when using such a method for future dating exercises. Finally, using this type of markers for NGRIP in a 5 cores dating exercise with Datice, we show that the new ice core chronologies obtained with these markers do not differ by more than 410 years from AICC2012 for Antarctic ice cores and 150 years from GICC05 for NGRIP over the last 60 thousand years.

1 Introduction

The reference timescale for Greenland ice cores, GICC05, has been obtained by layer counting back to 60 ka (thousands of years before present, present being year 1950 all along our study; Vinther et al., 2006; Rasmussen et al., 2006; Andersen et al., 2006; Svensson et al., 2008). This chronology is absolute with an increasing associated uncertainty with depth, reaching more than 2.6 ka at 60 ka. Because this chronology is based on annual layer counting, the duration of events is rather precise, even for old ages, with an uncertainty of about 0–4 years for counting of 20 annual layers. Since the layer counting is not independent from one interval to another, the

final uncertainty on the GICC05 chronology cumulates the counting error (Maximum Counting Error (MCE); Rasmussen et al., 2006).

This chronology has been used as a reference for many records of the North Atlantic region (Austin et al., 2012; Walker et al., 2012; Austin and Hibbert, 2012; Davies et al., 2012; Blockley et al., 2012b). It has also been used as a basis over the last 60 ka for the recent construction of the coherent Antarctic Ice Core Chronology (AICC2012) gathering one Greenland ice core (NorthGRIP - NGRIP) and 4 Antarctic ice cores (EPICA Dome C - EDC, EPICA Dronning Maud Land - EDML, Talos Dome ice core - TALDICE and Vostok) (Bazin et al., 2013; Veres et al., 2013). For the construction of AICC2012 with the bayesian tool Datice (Lemieux-Dudon et al., 2010), we have imposed a 1–sigma deviation for NGRIP of 50 years maximum. Even if such a constraint is artificially too strong compared to the true uncertainty of GICC05, it permits to keep a coherency within 5 years between the NGRIP AICC2012 chronology and GICC05.

Still, the strong tie of AICC2012 to GICC05 had raised some technical problems when optimizing the chronology with the bayesian tool Datice. Three glaciological parameters are indeed optimized during this process: accumulation rate, ice thinning and lock–in depth (i.e. the depth at which air is trapped when snow is sufficiently compacted). The bayesian approach imposes to start with first guess (background) scenarios for the three parameters. They are then modified within their imposed variance range so that the final chronology fits the absolute and relative age constraints for each ice core within error bars.

In practice, to force the NGRIP AICC2012 chronology to fit the GICC05 age scale, we had to use the modeled thinning function and accumulation rate adapted to the GICC05 chronology (hereafter DJ–GICC05 scenarios; Vinther et al., 2006; Rasmussen et al., 2006; Andersen et al., 2006; Svensson et al., 2008) as background thinning and accumulation rate scenarios in Datice. In addition to absolute markers placed every 60 years with a maximum uncertainty of 50 years for the NGRIP ice core, the variance associated with the background scenarios of this ice core were imposed to be very small to prevent any deviation from the GICC05 timescale.

Even if the uncertainty of the GICC05 timescale is well constrained, this is not true for the DJ–GICC05 scenarios of thinning and accumulation. The thinning function is deduced from a simple Dansgaard–Johnsen (DJ) ice flow model (Dansgaard and Johnsen, 1969; Andersen et al.,

2006) that has been parameterized to obtain the best match between the modeled and observed depth–age horizons in the ice cores. Then, the thinning function calculated with the DJ model is used together with the observed annual layer thicknesses to produce an accumulation rate history. No uncertainty value is associated with the reconstructions of thinning and accumulation rate in Greenland ice cores but thinning reconstructed from such 1D ice flow model are only a first approximation (Cutler et al., 1995; Parrenin et al., 2004, 2007).

Recently, studies combining air isotopic measurements ($\delta^{15}\mathrm{N}$ of N_2) with firnification models have suggested that, both in NGRIP and NEEM, the accumulation rates reconstructed from the GICC05 or ss09sea chronologies, through layer counting and the DJ flow model, were overestimated during the last glacial period (Huber et al., 2006; Guillevic et al., 2013; Kindler et al., 2014). Indeed, $\delta^{15}\mathrm{N}$ of N_2 of air trapped in an ice core indicates the depth and the amplitude of abrupt temperature changes in the gas phase through thermal fractionation. The depth difference between the same abrupt temperature changes recorded in the ice phase through ice $\delta^{18}\mathrm{O}$ increase/decrease and in the gas phase through a positive/negative $\delta^{15}\mathrm{N}$ peak is called delta–depth (Δdepth). Moreover, in the absence of any abrupt temperature change and convection at the top of the firn, the $\delta^{15}\mathrm{N}$ gives an indication of the past lock–in depth (LID) due to gravitational fractionation. A firnification model including heat diffusion and mainly driven by temperature and accumulation rate can reproduce long term and abrupt $\delta^{15}\mathrm{N}$ variations with depth for Greenland ice cores. The same would not be true in Antarctica where a strong discrepancy between firnification models and data is observed (Landais et al., 2006; Capron et al., 2013). Still, it has been shown that the $\delta^{15}\mathrm{N}$ profile is best reproduced when the ss09sea accumulation rate for NGRIP is decreased by $\sim 20\%$ over the period 20 to 60 ka (Kindler et al., 2014; Huber et al., 2006).

It thus appears that the way NGRIP was implemented in the Datice tool for the AICC2012 chronology is not optimal. In addition to GICC05 chronological uncertainties that were not taken into account by construction, imposing the DJ–GICC05 accumulation rate and thinning scenarios with artificially reduced variances most probably led to incorrect output scenarios for these glaciological parameters.

In this paper, we propose an improvement of Datice to better implement the chronological uncertainties. We incorporate the possibility of integrating markers of age–difference and

propose different way to transfer the counting error of each interval to the global chronology uncertainty. This permits to relax the strong constraints on thinning and accumulation rate and allow the NGRIP chronology to differ from GICC05 chronology within its error bars.

The outline of the manuscript is the following. In a first methodological section, we present and validate the improvement made on the Datice tool in order to integrate the markers of age–difference with their uncertainties. Then, we discuss different ways to implement the counted errors within the global chronological uncertainty. We also present some sensitivity experiments with the modified Datice tool for optimizing the sampling strategy and correlation between counted errors. Finally, we focus on how this new version of Datice modifies the NGRIP and the 4 Antarctic ice cores chronologies compared to AICC2012.

2 Implementation of constraints from counted layers in Datice

2.1 Methodology

The purpose of the following section is to describe the modifications implemented in Datice (Lemieux-Dudon et al., 2009, 2010) to take account of an additional constraint : the markers of age–difference. This type of marker enables one to constrain the duration over depth intervals along ice cores. This constraint is applied by feeding Datice with the beginning and end depths of the interval, its duration, the duration uncertainty, and optionally the error correlation between markers.

Datice aims at obtaining the best age model scenario by formulating an optimization problem with a cost function that is accounted for by two main types of constraint: the paleo–observations $\boldsymbol{Y}$ and a first guess age model $\boldsymbol{X}^b$ (referred to as the prior or **background**). A strong requirement is the independence between the background age model and the paleo–observations, since the the cost function J is derived from the Bayes theorem:

$$J(\boldsymbol{X}) = -\log\left(P(\boldsymbol{Y}|\boldsymbol{X})\, P_b(\boldsymbol{X})\right) \tag{1}$$

where $P(\boldsymbol{Y}|\boldsymbol{X})$ and $P_b(\boldsymbol{X})$ are the likelihood and prior probability distribution Tarantola (2005).

In practice, Datice is applied to several ice cores with large set of paleo–observations, to calculate coherent chronologies for both the ice and gas phases. The chronologies are deduced (Appendix A) from the scenarios of three glaciological parameters : (i) T_k the total thinning function, (ii) A_k the accumulation rate, and (iii) C_k the lock–in depth in ice equivalent (LIDIE). To run a Datice simulation, paleo–observations and background parameters $T_k^b(z)$, $A_k^b(z)$ and $C_k^b(z)$ must be provided to Datice with their respective uncertainties. The optimization of the cost function J enables to refine the background by identifying correction functions $\tau_k(z)$, $\alpha_k(z)$ and $\gamma_k(z)$ at each depth level z_k, for each core indexed with k:

$$T_k(z) = \tau_k(z) \cdot T_k^b(z) \tag{2}$$

$$A_k(z) = \alpha_k(z) \cdot A_k^b(z) \tag{3}$$

$$C_k(z) = \gamma_k(z) \cdot C_k^b(z) \tag{4}$$

From a particular set of correction functions, one can deduce a particular age model. Hereafter, we set $\boldsymbol{X} = (\boldsymbol{\alpha_k}, \boldsymbol{\tau_k}, \boldsymbol{\gamma_k})^T$.

The Datice cost function formulation (equation 5) relies on the following important statistical assumptions. In the prior probability distribution of equation 1, the parameters T_k, A_k and C_k are supposed to be independent and lognormally distributed, with medians set equal to the background $T_k^b(z)$, $A_k^b(z)$ and $C_k^b(z)$. The prior probability distribution is further rewritten in terms of the correction functions (equations 2, 3 and 4), to which we apply the change of variable $\tilde{\boldsymbol{X}} = \log(\boldsymbol{X})$ in order to transform lognormal into normal probability distributions (pdf; Tarantola, 2005). Since observations of different types are supposed to be independent with either normal or lognormal distributed errors, the likelihood of Appendix 1 is itself a product of normal pdfs. Under these assumptions, the cost function J sums up quadratic terms (equation 5).

Until now, observation $\boldsymbol{Y}$ could be of the following types: ice and gas age markers (^{ia} and ^{ga}), delta-depth markers (^{dd}), or ice and gas stratigraphic links (^{is} and ^{gs}) (Lemieux-Dudon

et al., 2010; Buiron et al., 2011; Veres et al., 2013; Bazin et al., 2013). The application of the markers of age–difference (^{ad}) leads to an additional term in the cost function (equation 5), with special care to preserve the Datice hypothesis of no error correlation between (i) observations of different types, (ii) observation of different cores, or (iii) observation and background model scenarios:

$$
\begin{aligned}
J(\tilde{\boldsymbol{X}}) = & \sum_{k=1}^{N} \left(\tilde{\boldsymbol{X}}_k - \tilde{\boldsymbol{X}}_k^b \right)^T [\mathbf{B}]^{-1} \left(\tilde{\boldsymbol{X}}_k - \tilde{\boldsymbol{X}}_k^b \right) \\
& + \sum_{k=1}^{N} \left(\boldsymbol{Y}_k^{dd} - \mathbf{h}_k^{dd}(\tilde{\boldsymbol{X}}_k) \right)^T [\mathbf{R}_k^{dd}]^{-1} \left(\boldsymbol{Y}_k^{dd} - \mathbf{h}_k^{dd}(\tilde{\boldsymbol{X}}_k) \right) \\
& + \sum_{k=1}^{N} \left(\boldsymbol{Y}_k^{ia} - \mathbf{h}_k^{ia}(\tilde{\boldsymbol{X}}_k) \right)^T [\mathbf{R}_k^{ia}]^{-1} \left(\boldsymbol{Y}_k^{ia} - \mathbf{h}_k^{ia}(\tilde{\boldsymbol{X}}_k) \right) \\
& + \sum_{k=1}^{N} \left(\boldsymbol{Y}_k^{ga} - \mathbf{h}_k^{ga}(\tilde{\boldsymbol{X}}_k) \right)^T [\mathbf{R}_k^{ga}]^{-1} \left(\boldsymbol{Y}_k^{ga} - \mathbf{h}_k^{ga}(\tilde{\boldsymbol{X}}_k) \right) \\
& + \sum_{k=1}^{N} \left(\boldsymbol{Y}_k^{is} - \mathbf{h}_k^{is}(\tilde{\boldsymbol{X}}_k) \right)^T [\mathbf{R}_k^{is}]^{-1} \left(\boldsymbol{Y}_k^{is} - \mathbf{h}_k^{is}(\tilde{\boldsymbol{X}}_k) \right) \\
& + \sum_{k=1}^{N} \left(\boldsymbol{Y}_k^{gs} - \mathbf{h}_k^{gs}(\tilde{\boldsymbol{X}}_k) \right)^T [\mathbf{R}_k^{gs}]^{-1} \left(\boldsymbol{Y}_k^{gs} - \mathbf{h}_k^{gs}(\tilde{\boldsymbol{X}}_k) \right) \\
& + \sum_{k=1}^{N} \left(\boldsymbol{Y}_k^{ad} - \mathbf{h}_k^{ad}(\tilde{\boldsymbol{X}}_k) \right)^T [\mathbf{R}_k^{ad}]^{-1} \left(\boldsymbol{Y}_k^{ad} - \mathbf{h}_k^{ad}(\tilde{\boldsymbol{X}}_k) \right)
\end{aligned}
\tag{5}
$$

In equation 5, the first term measures how far is the current age model $\tilde{\boldsymbol{X}}$ from the background scenarios $\tilde{\boldsymbol{X}}^b$. The six following terms are related to the observation constraint, and measure the distance between the observations $\boldsymbol{Y}$ and the current age model $\tilde{\boldsymbol{X}}$. Importantly,

to map the current age model $\tilde{\boldsymbol{X}}$ to the observation $\boldsymbol{Y}$, we must introduce the non linear observation operators $\mathbf{h}$. The background and observations uncertainties provided to Datice are stored in the background and observation error covariance matrices $\mathbf{B}$ and $\mathbf{R}$ (Appendix D1). The cost function terms are weighted according to the uncertainties specified in the $\mathbf{B}$ and $\mathbf{R}$ matrices. The cost function reaches a minimum value for a specific set of correction functions $\tilde{\boldsymbol{X}}^a$ (equations 2, 3 and 4). At this minimum, a trade-off is reached between the background and observation constraints. The new age scales, hereafter called **analysed chronologies** are then deduced from the correction functions $\tilde{\boldsymbol{X}}^a$ (Appendix A). By propagating the errors stored in the $\mathbf{B}$ and $\mathbf{R}$ matrices, Datice estimates the error associated with the age solution (Appendix D2). We refer to this error as the **analysed error**. Both the analysed age scales and analysed errors are highly sensitive to the errors specified in the $\mathbf{B}$ and $\mathbf{R}$ error covariance matrices.

In this article, we wish to design Datice simulations with markers of age–difference derived from the GICC05 counted layer chronology. In section 2.3, we especially investigate how to set the observation error covariance matrix $\mathbf{R}^{ad}$ associated with these markers:

$$\mathbf{R}_{ij}^{ad} = \rho_{ij}^{ad} \sigma_i^{ad} \sigma_j^{ad} \tag{6}$$

where $\mathbf{R}_{ij}^{ad}$ accounts for the error covariance between the i$^{\text{th}}$ and j$^{\text{th}}$ pair of markers Y_i^{ad} and Y_j^{ad}, which are applied in the Datice system. σ_i^{ad} and σ_j^{ad} are their standard deviations and ρ_{ij}^{ad} their error correlation coefficient.

2.2 Validation of Datice developments: twin experiments

In this section, we construct twin experiments in order to test the extension of the Datice tool with markers of age–difference. Twin experiments enable one to test any data assimilation system. It consists first in the construction of some synthetic data and background by applying random perturbations of known statistical distribution to a given model scenario. The unperturbed model scenario is refereed as the "truth". The aim of this validation method is to rebuild the truth by running the data assimilation system on the perturbed data and background.

In our case, we have designed 51 experiments where Datice is run with only the NGRIP ice core. The GICC05 age scale is considered as the truth. The only observation included in Datice for these experiments are the markers of age–difference. The ice chronology construction will thus be constrained on one hand by the perturbed annual layer counting from GICC05, and on the other hand by the thinning and accumulation rate scenarios with associated uncertainties.

Each twin experiment inputs are prepared using the following method. First, we sample markers of age–difference from the GICC05 age scale every 100 years and we derive their associated errors based on the MCE with the assumption of full correlation (i.e. the counting errors for each annual layer within the 100 years interval are cumulated, see section 2.3). For this experiment, the markers $\boldsymbol{Y}^{ad,t}$ represent the "truth" (superscript t) as extracted from the reference model age GICC05. These "true" markers are then perturbed within their uncertainty range through random normal perturbations constructed in each twin experiment, according to $\mathbf{R}^{ad}$ the observation error covariance matrix (see section 2.1), to provide the makers of age–difference $\boldsymbol{Y}^{ad}$ that will be effectively applied in the simulations:

$$\boldsymbol{Y}^{ad} = \boldsymbol{Y}^{ad,t} + \boldsymbol{\delta}^{ad} \quad \text{with} \quad \boldsymbol{\delta}^{ad} \sim \mathcal{N}\left(0, \mathbf{R}^{ad}\right) \tag{7}$$

We then construct the 51 background scenarios symmetrically. We apply some random log-normal perturbations to the GICC05 thinning function T_i^t and accumulation rate A_i^t at each depth level z_i (with index i running from 1 at the top of the core to N at the bottom), which can be arranged in the two following vectors:

$$\boldsymbol{\delta}_\alpha = (\delta_1^\alpha, \ldots, \delta_i^\alpha, \ldots, \delta_N^\alpha) \tag{8}$$

$$\boldsymbol{\delta}_\tau = (\delta_1^\tau, \ldots, \delta_i^\tau, \ldots, \delta_N^\tau) \tag{9}$$

These vectors are applied as multiplicative factors on the true model scenarios (superscript t) to give the perturbed backgrounds (superscript b, equations 10 and 11).

$$T_i^b = \delta_i^\tau \, T_i^t \tag{10}$$

$$A_i^b = \delta_i^\alpha \, A_i^t \tag{11}$$

The logarithm of vectors $\boldsymbol{\delta}^\tau$ and $\boldsymbol{\delta}^\alpha$ are distributed with a multivariate normal probability density function of zero mean and covariances set by the background error covariance matrices $\mathbf{B}_\tau$ and $\mathbf{B}_\alpha$:

$$\log\left(\boldsymbol{\delta}^\tau\right) \sim \mathcal{N}\left(0, \mathbf{B}_\tau\right) \tag{12}$$

$$\log\left(\boldsymbol{\delta}^\alpha\right) \sim \mathcal{N}\left(0, \mathbf{B}_\alpha\right) \tag{13}$$

where $\mathbf{B}_\alpha$ and $\mathbf{B}_\tau$ are the first two diagonal and decorrelated blocks of matrix $\mathbf{B}$ introduced in equation 5 of section 2.1.

For all twin experiments, the $\mathbf{B}_\alpha$ and $\mathbf{B}_\tau$ matrices are constructed accordingly to Bazin et al. (2013) with adapted values (see Table 3 and Appendix B).

Figure 1 shows the large spread of the resulting perturbed background age scales (dashed lines) and a superimposition of the corresponding analysed age scales (orange lines). Figure 2 shows the difference between the set of analysed chronologies minus GICC05 (upper panel) and the error of the analysed chronologies, σ^a, the *a posteriori* standard deviation as calculated by Datice (lower panel). Histograms of the background and analysed chronologies are shown on Figure 3 for the 1800m depth level.

One can observe that the perturbed background age scales spread toward larger values when older than GICC05, which confirms the expected disymmetry of their probability distribution. In the Datice system, the calculation of the analysed error σ^a is based on the assumption of normally distributed errors, which may be a strong assumption. However the set of analysed chronologies rather constitutes a symmetric distribution centered on GICC05 (a larger number of samples might help to refine this analysis). Taking as a reference the output chronology error σ^a at 1800 m, 96% of the samples are inside a $\pm 2\,\sigma^a$ envelop (see histogram of Figure 3), which gives confidence in the estimate of the analysed error.

Finer diagnostics confirm the reliability of the Datice methodological developments. On the basis of ensemble of analyses conducted on ensemble of perturbed background and observations, several levels of *a posteriori* diagnostics can be applied on data assimilation system as investigated in Desroziers et al. (2009). The construction of the twin experiments appropriately relies on an ensemble of both perturbed background and observations. It consequently enables one to verify the level one of these diagnostics. It states that for weakly non linear observation operators $\mathbf{h}$ (see equation 5, section 2.1), when both the $\mathbf{B}$ and $\mathbf{R}$ matrices are calibrated, averaging the values of the cost function at the optimum (when $\boldsymbol{X}^a$ optimum is reached) must be equal to the number of observations p:

$$\mathbf{E}\left[J\left(\tilde{\boldsymbol{X}}^a\right)\right] = p \tag{14}$$

In our set of twin experiments, we apply 633 markers of age–difference. The average of our cost function at optimum $\tilde{\boldsymbol{X}}^a$ over our 51 twin experiments gives 626. This is a quite fair result that validates our methodological development.

One should note that we have applied perfectly calibrated background and observation error covariance matrices. Indeed, the background and observation errors specified in the cost function are exactly the $\mathbf{B}$ and $\mathbf{R}$ matrices that have been used to produce synthetic background and observation data on the basis of the true scenario. In a more complex experiment, the $\mathbf{B}$ and $\mathbf{R}$ matrices are usually misspecified because the background and observation errors, $\tilde{\boldsymbol{\epsilon}}^b$ and $\boldsymbol{\epsilon}^o$, are usually poorly known since the truth itself is the unknown $\tilde{\boldsymbol{X}}^t$ (see Appendix D1). In such cases, the *a posteriori* diagnostics are applied to calibrate the error covariance matrices. In future work we wish to conduct such calibration on Datice experiments involving several ice cores.

2.3 Implementing layer counting error (MCE)

Layer counting consists in identifying annual cycles on the basis of annual layer proxies recorded along the core. The identification of annual cycles is subjected to errors. In order to deal with

uncertain annual layers and to derive a counting error estimate, GICC05 adopted the following statistical approach. If the ith annual cycle is identified as certain, the layer is counted as a full year with a zero error. Otherwise, for an uncertain ith annual cycle, the layer counts for half a year plus or minus half a year. For each annual cycle numbered with index i from top to 60 ka, one can introduce the two following variables n_i and σ_i in order to record the counting of layers and its error:

$$n_i \pm \sigma_i = 1 \pm 0\,\text{yrs} \qquad \text{For a certain layer} \tag{15}$$

$$n_i \pm \sigma_i = 0.5 \pm 0.5\,\text{yrs} \qquad \text{For an uncertain layer} \tag{16}$$

From the above layer counting data, one can infer duration measures along the core by summing up the n_i cycles. For instance between depths z_q and z_p, delimiting the start and the end of the qth and pth annual cycles respectively, the duration Y_{z_q,z_p} in years writes:

$$Y_{z_q,z_p} = \sum_{i=q}^{p} n_i \tag{17}$$

The official GICC05 age scale provides the counting data and error cumulated over time windows of 20 years. The GICC05 error estimate is called the Maximum Counting Error or MCE. It sums up the error of the individual cycles (i.e., σ_i) over the corresponding time window. The official file records these data for the successive depths interval $[z_q, z_p]$ back to 60 ka:

$$Y^{20yrs}_{z_q,z_p} = \sum_{i=q}^{q+19} n_i = 20\,\text{yrs} \tag{18}$$

$$\text{MCE}^{20yrs}_{z_q,z_p} = \sum_{i=q}^{q+19} \sigma_i \tag{19}$$

For our experiments, our objective is to apply the GICC05 measure of duration Y_{z_q,z_p}^{20yrs} as markers of age–difference in Datice simulations. Two questions arise at this stage:

- Over which time window should we sample the GICC05 makers of age–difference?
- How should we infer the associated error?

None of these questions are trivial ones. They are closely interlinked through the existence of error correlation between annual layers and the assumptions inherent to the MCE construction.

One way to better understand the MCE is to reformulate the GICC05 counting process with two normal probability density functions (pdf): (i) the pdf of annual cycles identified as **certain** with a 1–year mean and a variance that tends to zero (ii) the pdf of annual cycles identified as **uncertain** with a mean and standard deviation both set to half a year. This formalism is questionable and some issues are addressed in Appendix C1. Under this formalism, the calculation of the error Σ_{z_q,z_p} on any counting measure Y_{z_q,z_p} is well-documented, and the role played by the error correlation between annual cycles n_i and n_j becomes quite clear. If ρ_{ij} records such correlation, the Σ_{z_q,z_p} error writes:

$$\Sigma_{z_q,z_p}{}^2 = \sum_{i=q}^{p} \sigma_i{}^2 + 2 \sum_{i=q}^{p} \sum_{j=q,j>i}^{p} \rho_{ij} \sigma_i \sigma_j \tag{20}$$

The Σ_{z_q,z_p} error reaches a minimum value in the case of a null error correlation between any pair of cycles (i.e., $\rho_{ij} = 0$):

$$\mathrm{Min}\left[\left(\Sigma_{z_q,z_p}\right)^2\right] = \sum_{i=q}^{p} \sigma_i{}^2 \tag{21}$$

On the contrary, the error reaches a maximum value when the error correlation between annual cycles is maximum (i.e., $\rho_{ij} = 1$):

$$\mathrm{Max}\left[\left(\Sigma_{z_q,z_p}\right)^2\right] = \sum_{i=q}^{p} {\sigma_i}^2 + 2\sum_{i=q}^{p}\sum_{j>1,j=q}^{p} \sigma_i\sigma_j = \left(\sum_{i=q}^{p}\sigma_i\right)^2 \tag{22}$$

The MCE formulation shown in equation 19 is explained by equation 22. It assumes a full error correlation between any pair of measured annual cycles regardless of their respective position along the core. The terminology is well-chosen since the MCE error is an upper estimate of the error regarding the value of the correlation coefficient (but not regarding the assumptions on the error σ_i).

The MCE calculation of GICC05 results at each depth level in the sum of the MCE of every duration interval from the top to the considered depth level. Still, the authors have acknowledged that the assumption of full correlation of counting errors along the ice core is not correct and stated that "recognizing that the counting errors in reality are neither uncorrelated nor fully correlated, we adopt the simple and conservative approach, summing up the uncertainties as if they were correlated" (Rasmussen et al., 2006). Consequently, the 1-sigma uncertainty of the GICC05 ice core is considered as half the MCE.

The MCE formulation assumes error correlation on an "infinite range" along the core (ρ_{ij} does not decrease with the distance between the measured cycles). In reality, the error correlation does not have an infinite range. Moreover, as depicted in Appendix C2, the errors associated with age markers may be linked to the sampling rates and we discuss briefly below the possible implications for choosing a sampling rate of 20 or 40 years. While for the 20 years sampling, we may straightforwardly implement the 20yrs-window markers ($Y^{20yrs}_{z_q,z_p}$) and errors ($\mathrm{MCE}^{20yrs}_{z_q,z_p}$) from GICC05, different extreme views can be proposed for a 40 years sampling:

1. Either we believe that the full error correlation assessed over the 20yrs time-window between annual layers cuts-off. Then, no correlation exists between the annual cycles included in the two separated but adjacent depth intervals $[z_q, z_p]$ and $[z_p, z_m]$. Under this assumption, the theory shows that we must sum up the squared 20yrs MCE errors:

$$\mathrm{MCE}_{z_p,z_m}^{40yrs} = \sqrt{\left(\mathrm{MCE}_{z_q,z_p}^{20yrs}\right)^2 + \left(\mathrm{MCE}_{z_p,z_m}^{20yrs}\right)^2} \tag{23}$$

2. On the opposite, we believe that the full error correlation assessed over the 20yrs time-window between annual layers extends over the 40yrs time-window (which means over the depth interval $[z_q, z_m] = [z_q, z_p] \cup [z_p, z_m]$). In that case the theory shows that we must sum up the 20yrs MCE errors:

$$\mathrm{MCE}_{z_p,z_m}^{40yrs} = \mathrm{MCE}_{z_q,z_p}^{20yrs} + \mathrm{MCE}_{z_p,z_m}^{20yrs} \tag{24}$$

From this simple illustration, it follows that markers of age–difference and errors sampled on GICC05 at different rates (i.e., 40-60-80-100 years...), derived by summing-up the GICC05 20yrs-window MCE error must be understood as very distinct inputs and different simulation outputs must be expected. This is not fully satisfactory for the age scale construction and associated error estimates since we do not want to give so much weight to the rather arbitrary choice of the sampling rate. In order to separate the problems of error correlation and sampling in our approach, we have thus included the possibility in the Datice approach to apply error correlation on a finite interval and avoid abrupt cut-off of error correlation between adjacent intervals. This development should permit to sample the markers at a 40 years step and apply error correlations beyond the 40yrs-window interval. Indeed, we expect that the value of the error correlation may change along the core, for instance with the climatic periods and changes in annual layers thickness.

For this formulation of error correlation on a finite range, the correlation coefficients ρ_{ij}^{ad} of the observation error covariance matrix $\mathbf{R}^{ad}$ (equation 6) are set according to a correlation function f that smoothly decreases with the distance between two markers of age–difference Y_i^{ad} and Y_j^{ad}:

$$\rho_{ij}^{ad} = f\left(|z_i^{ad} - z_j^{ad}|\right) \tag{25}$$

The shape of the function f is chosen as the product of a gaussian and a triangular function:

$$f\left(|z_i^{ad} - z_j^{ad}|\right) = \exp\left(-\frac{\left(z_i^{ad} - z_j^{ad}\right)^2}{2\,L^{ad2}}\right)\left(1 - \frac{|z_i^{ad} - z_j^{ad}|}{2\,L^{ad}}\right) \tag{26}$$

where L^{ad} must be set in meters in order to adjust the width of the f function and therefore the scope of the error correlation. The larger L^{ad} is, the more correlation between markers of age–difference.

With this new formulation of the error correlation, we can explore how both sampling and error correlation independently affect the final chronology and provide some guidelines for future dating exercises.

2.4 Tests and optimization of the Datice system to apply the GICC05 markers of age–difference

In the following section, we extract several sets of markers of age–difference from GICC05, with different sampling and/or different assumptions regarding the associated error. We conduct multiple Datice simulations with these inputs in order to investigate the sensitivity of the solution to the markers sampling and errors.

In this respect, we designed several experiments ran on the NGRIP core alone, with only markers of age–difference as constraints. Details on the background settings are provided in Table 3. Still, it should be noted that in these experiments we kept the 1 m resolution used in multi–cores experiments such as AICC2012. On such a depth grid, the annual layer thickness drops below 0.05 meter per year at some depth level so that the number of years in a 1 meter layer becomes larger than 20 years. Datice cannot handle markers of age–difference that are sampled below the depth grid resolution. This technical issue render impossible to apply the GICC05 20yrs-window markers and MCE errors directly. For that reason, we propose an adaptive sampling ranging between 40 and 140 years back to 60 ka, which is designed to prevent the markers to be sampled below the 1 m resolution.

2.4.1 Sampling influence

To study the influence of sampling we run three experiments with markers sampled at three uniform rates (100, 200 and 300 years) as well as the experiment with an adaptive sampling between 40 to 140 yrs. The associated errors for the 3 uniform sampling are derived from the 20yrs-window MCE data under the assumption of full error correlation between annual cycles over the length of the interval, hereafter **AddMCE** assumption. For the experiment with the adaptive sampling, we test errors derived in the full correlation assumption as well as errors with abrupt cut-off of correlations beyond 20yrs-windows, hereafter **SqrAddMCE** assumption. The terminology AddMCE and AddSqrMCE refers to equations 24 and 23, where in the former case the MCE errors are added, while in the latter case the squared MCE errors are added. Table 1 summarizes the experiment configurations.

Figures 4 and 5 show the different NGRIP simulations. As expected and discussed in section 2.3, the age solutions and their associated errors are sensitive to the sampling. In the comparison of the four experiments ran in the AddMCE assumption, we better reproduce the GICC05 details with finer sampling rates, e.g., 40yrs vs 200yrs (5). Still, finer sampling of the markers of age–difference is not directly the reason for the better agreement with GICC05. Indeed, as error correlations are cumulative in the AddMCE assumption, the observation error largely increases with the length of the marker sampling window. Consequently, the strength of the marker constraint reduces, which deteriorates the convergence toward GICC05. The observation error impact is also illustrated in Figure 4 when comparing the two adaptive sampling simulations. The simulation run with the assumption of abrupt correlation cut-off beyond 20 years (SqrAddMCE) better converge toward GICC05 with a smaller associated error. Again, different observation errors are obtained under the different assumptions of error correlation. The SqrAddMCE assumption strongly reduces the observation error at any depth along the core with respect to the full correlation assumption.

Option SqrAddMCE may therefore be a way to relax the dependence of the analysed error to the sampling. However, as mentioned above, the abrupt correlation cut-off may be questioned. At the junction of two markers of age–difference, neighboring annual cycles from either sides

does not share any error correlation while each of them correlates with much further layers (as long as these layers are included in the marker time window). We actually rather expect error correlations to smoothly decrease with the distance between annual cycles.

We have demonstrated the sensitivity of the solution to the sampling and to the MCE error assumptions applied to derive the observation error. Both issues were however not fully decoupled in this first illustration. We thus investigate in the next section possible ways to study the error correlation independently from the sampling.

2.4.2 Influence of error correlation

In this section, we apply different correlation coefficients between markers of age–difference as implemented in Datice (equations 6 and 25). This methodological implementation enables one to study the influence of error correlation independently of the sampling. In the following experiments, we investigate two correlation configurations: (i) correlation coefficients with infinite depths range along the core, hereafter **InfiniteRangeCorr**, (ii) correlation coefficient smoothly decreasing with the distance between markers, hereafter **FiniteRangeCorr**.

In this set of experiments, the level of observation error is largely increased for large correlation coefficient values. To operate with configurations where the minimization and solution are still strongly driven by the constraint of the markers of age difference, the background errors have been exaggerated (Table 3). In such configuration, the analysed error should tend toward the observation error (Appendix E1):

$$\sigma_b \gg \sigma_o \implies \sigma_a \sim \sigma_o \tag{27}$$

where σ_b, σ_o and σ_a are the background, the observation and the analysed errors, respectively.

In a first set of simulations, we investigate the **InfiniteRangeCorr** option. The correlation coefficient ρ_{ij}^{ad} (equation 25) is set to constant values ranging from 0.2 to 0.8. Such configuration implies identical error correlations between markers separated by a large or a small distance as the MCE formulation does for the GICC05 chronology. Actually, the MCE formulation implies a correlation coefficient of 1 all along the ice core. In the Datice approach, it is technically

impossible to attribute a value of 1 to ρ_{ij}^{ad} due to the $\mathbf{R}^{ad}$ matrix inversion in the cost function formulation (equation 5). As a consequence, the Datice experiment run with a correlation coefficient of 0.8 is the closest analog to the MCE formulation and we expect the analysed error to closely approach the MCE.

Figure 6 show a comparison of the background and analysed chronologies with the reference chronology GICC05 as well as the Datice analysed errors and the MCE. As expected, the analysed errors tend toward the MCE for higher correlation coefficients. The full convergence to the MCE error values is however hampered since more error correlation between markers progressively rules out the hypothesis of equation 27: when the observation error becomes too large, the analysed error is also driven by the background error (equation E11). Analysed chronologies also show some predictable behavior. When the correlation coefficient increases, the confidence in the markers of age–difference decreases and the analysed chronologies stay close to the background chronologies. At last, the reconstructed chronologies show an increasing bias relatively to GICC05 with increasing correlation coefficient. In the 0.8 correlation coefficient case, the bias is close to 40 years at 1900 m, and reaches 90 years at 2000 m. At shallower depths, the bias strongly decreases (a few years at 500 m). This can be explained by the lesser amount of uncertain layers, which are the only layers contributing to the error correlation (layers identified as certain have a zero σ_i error and do no contribute to covariance of errors in equation 20).

We test hereafter the **FiniteRangeCorr** experiment with the finite depth range correlation coefficient. We ran simulations with five different type of sampling: (i) four uniform sampling rates (300, 200, 100 and 80 years) and (ii) the adaptive sampling 40–140yrs. The markers errors are systematically derived under the AddMCE assumption. An error correlation is applied between markers (equation 25), and for all experiments we have set the correlation length L^{ad} to 300 years (equation 26).

Figure 7 shows a comparison between background, analysed chronologies and GICC05 as well as analysed errors. We clearly observe that there is a good fit to GICC05 with a better resemblance for the highest sampling rate, as expected and already observed in previous sections. Importantly, despite the different sampling rates, the analysed errors show very similar values contrary to tests presented in the previous section. This is due to the fact that the analysed er-

ror is mainly influenced by the correlation coefficient on a finite length, which inter–correlates more efficiently markers sampled on short time-windows.

Summarizing, the tests presented in the two previous sections suggest some guidelines for future constructions of chronology using the markers of age–difference. The central problem is the definition of the error associated with annual layer counting and how this error is correlated with other layers errors. We have seen that making different assumptions on the error correlation lead to significant difference in the final chronology and associated error. In simulations with Datice applied to several ice cores including NGRIP, if the objective is to preserve the NGRIP age scale, our recommendations are: (i) sample the markers of age–difference over small time windows (e.g. 100 years or apply an adaptive sampling rate), (ii) use a small uncertainty for the observations (this is directly linked to a large or short range of correlation between layer counting errors), or (iii) increase the NGRIP overall background error.

3 Application to 5 sites experiments and comparison with AICC2012

After having validated the new developments for the implementation of markers of age–difference and possible error correlation, we show a first application of the new Datice tool to a 5 ice core experiment (NGRIP, EDC, EDML, Vostok, Taldice).

An important condition to use Datice properly is to respect the independence between the age constraints and the background scenarios. This was not the case when building AICC2012 for the NGRIP ice core. Here, the new development of Datice allows one to use scenarios for background accumulation rate and thinning function independent from the age constraints deduced from GICC05 for NGRIP. In this application, the thinning function is the same as for AICC2012, obtained from the 1D–DJ glaciological model adapted to NGRIP (Andersen et al., 2006). However, we have largely increased its associated variance to make it comparable to the ones associated with the background thinning function of the other cores implemented in Datice. For the accumulation rate, we use the ss09sea accumulation rate based on variations of water isotopes (Johnsen et al., 2001). An accumulation rate scenario is deduced from the water isotope profile corrected for the isotopic composition of seawater (e.g. Lorius et al., 1985). Then,

the relationship between the accumulation rate and the $\delta^{18}O$ profile is adjusted in order for the 1D–DJ ice flow model to match observed depth–age horizons. The formulation and coefficients of the variance of NGRIP background accumulation rate are the same as in AICC2012 and comparable to other ice cores. The LIDIE background scenario in AICC2012 was built from a firnification model (Goujon et al., 2003) whose input parameters (temperature and accumulation rate) were roughly adjusted to be coherent with the mean $\delta^{15}N$ values measured over the NGRIP ice core. It was thus independent from GICC05 and has been kept unchanged for our study.

Concerning the age constraint, the absolute age markers deduced from GICC05 were replaced by markers of age–difference. The markers of age–difference are obtained from the GICC05 chronology with adaptive length of intervals between 40 and 140 years with the AddMCE assumption (full correlation between annual cycles) and a correlation length of 300 years. In order to constrain the relative gas chronology vs the ice chronology, we use information derived from $\delta^{15}N$ of air trapped in ice bubbles. New $\delta^{15}N$ data on the NGRIP ice core have been published since the AICC2012 chronology (Kindler et al., 2014). In particular, these data permit to identify depths of rapid temperature increases associated with the beginning of Greenland Interstadials (GI) 1 to 7 in the gas phase. The depth differences between peaks of $\delta^{18}O_{ice}$ and $\delta^{15}N$ of a concomitant event recorded in the ice and the gas phases are thus used as delta–depth (Δdepth) constraints. With the new set of data from Kindler et al. (2014), we were thus able to deduce new Δdepth markers that were not available for the construction of AICC2012 (Table 2). Their uncertainties depend on the resolution of measurements and the difference of Δdepth estimates. Indeed, the Δdepth can be estimated from the difference between mid-slopes of $\delta^{18}O_{ice}$ and $\delta^{15}N$ increases or from the difference between the maxima of $\delta^{15}N$ and $\delta^{18}O_{ice}$.

Figure 8 compares this new Datice chronology (NGRIP-free) to AICC2012 for the 5 sites between 35 ka and 48 ka. We strengthen that the NGRIP-free chronology discussed here should not be taken as a new official chronology. It is only a test for our methodological development. Moreover, the AICC2012 chronology has the strong advantage of being in exact agreement with the GICC05 chronology and hence to facilitate the multi-archives comparison taking GICC05 as reference as already made in many studies (INTIMATE project: Blockley et al., 2012a). When

looking at the NGRIP ice records, the final NGRIP-free chronology does not differ from the GICC05 or AICC2012 chronologies by more than 150 years over the last 60 ka (Figure 8).

The Antarctic chronologies are not much modified compared to the AICC2012 chronologies. They all differ by less than 410 years from AICC2012 (Figure 8), which is well within the uncertainties of these chronologies (400–1000 years over this period). The small differences between the NGRIP-free and AICC2012 chronologies mean that the relationship between Greenland and Antarctic climate discussed with AICC2012 for the millennial scale variability of the last glacial period stays valid on NGRIP-free (Veres et al., 2013). We observe a classical seesaw pattern with Antarctic temperature increasing during the Greenland stadials, with a faster and shorter increase at EDML than at EDC (Figure 8).

4 Conclusions

The bayesian tool Datice used for the construction of coherent ice cores chronology has been improved and now enables one to consider the duration of events as dating constraints. This development is more coherent with the building of chronologies based on layer counting where the absolute error, defined as the Maximum Counting Error, increases with depth because of a cumulative effect. To account for the fact that the counted errors on each interval are neither fully correlated nor uncorrelated, we have also introduced the possibility to adjust correlation between age–difference errors. There is no unique way to define the correlation between errors of age–difference and future dating exercises may propose different correlation coefficients for layer counting performed at different periods (glacial vs interglacial times). We have thus presented here some sensitivity tests for the sampling and correlation of errors associated with markers of age–difference. These tests lead to general guidelines for future dating exercises including layer counting as absolute age constraints. For example, to best respect an ice core chronology based on layer counting, we would favor a high frequency sampling of markers of age–difference with a finite depth range correlation. Finally, the comparison of AICC2012 with the chronology obtained over 5 polar sites using the improved Datice tool incorporating markers of age–difference and associated correlation of errors shows differences of less

than 410 years over the last 60 ka, well within the uncertainties associated with the AICC2012 chronology. Huge efforts in annual layer counting were produced in the recent years for ice core chronologies, in particular for the Western Antarctic WAIS ice core (Members, 2013). Future dating exercises should thus benefit from the methodological development and validation of the bayesian tool presented in this study.

Appendix A: Datice age models

The Datice age models are derived from three key ice core quantities: the total thinning function $T(z)$, the accumulation rate $A(z)$ and the LIDIE $C(z)$. They allow to estimate the ice age chronology $\Psi(z)$ as follows:

$$\Psi(z) = \int_0^z \frac{D(z')}{T(z') \cdot A(z')} dz' \tag{A1}$$

with $D(z)$ being the relative density of the snow/ice material.

The gas chronology $\chi(z)$, is defined using Δdepth data, which measures the in–situ depth difference between ice and gas of the same age. The gas age is further calculated as the ice age of the layer situated at the depth $(z - \Delta depth)$.

$$\Delta depth(z) = C(z) \cdot T(z) \tag{A2}$$

$$\chi(z) = \Psi(z - \Delta depth(z)) \tag{A3}$$

A background age scenario $T^b(z)$, $A^b(z)$ and $C^b(z)$ as well as age constraints are required to run Datice. To optimize the gas and ice age scales, the specification of the background and age constraints uncertainties are further needed. Depending on the confidence assigned to the background and to the markers, Datice will modify more or less the initial background scenario.

Appendix B: Error specification in the Datice experiments

B1 Background variances changing with depth

Here we remind the formulations used to define the thinning function, accumulation rate and the LIDIE variances, since several coefficients were corrected in this study.

The standard deviation of the thinning function is defined as:

$$\sigma_T(z) = c_{T_1} + c_{T_2} \cdot \int^{z} \frac{D(z)}{T(z)} dz + c_{T_3} \cdot \frac{\sigma_{A,loc}}{\sigma_{A,loc}^{max}} \tag{B1}$$

where c_{T_1}, c_{T_2} and c_{T_3} are user defined constant parameters (c_{T_2} equals $c \cdot 0.1/H$ where H is the maximum depth of the input and c a user defined constant), $T(z)$ is the thinning function, $D(z)$ the relative density, $\sigma_{A,loc}$ the local standard deviation of accumulation and $\sigma_{A,loc}^{max}$ the maximum standard deviation of accumulation. The last term was implemented in order to increase the thinning variance during large climatic transitions since it has been suggested that the mechanical properties of ice can be modified in these periods. For the purpose of the tests performed in this study, we have corrected the c_{T_2} value (from 0.000016 to 0.000064) that was used for NGRIP when building AICC2012. This correction permits to have a coherent parameterization of the thinning variance for the 5 ice cores. Moreover, we have reduced the c_{T_1} values from 0.01 to 0.00001 in order to be closer to the 0 variance hypothesis at the surface for all sites. We have also divided by 2 the c_{T_3} values for all five sites. The other coefficients have the same values as used to build AICC2012 (SOM Bazin et al., 2013).

The standard deviation for the accumulation rate is:

$$\sigma_A(z) = \sigma_{b,A} \cdot \frac{\mid A_0 - A \mid}{\mid A_0 - A \mid_{max}} \cdot \left(1 + c_{A_1} \frac{z}{z_{max}}\right) \tag{B2}$$

with $\sigma_{b,A}$ being a reference standard deviation, A_0 is the mean Holocene accumulation rate, c_{A_1} is a constant parameter. The variance associated with the accumulation rate scenario thus

increases when the background accumulation rate strongly deviates from the Holocene value. The reason for such a parameterization is that the reconstruction of accumulation rate from water isotopes through the exponential law is semi-empirical and its extrapolation far from the present-day conditions may be problematic.

In order to avoid too small variances, a threshold value, σ_m, is implemented for each ice core. When σ_A is smaller than σ_m, then σ_A is recalculated as:

$$\sigma_A = \sigma_m \cdot \left(1 + c_{A_1} \frac{z}{z_{max}}\right) \tag{B3}$$

where σ_m represents the minimum values, defined by user.

We have kept the same values for all Antarctic sites for the $\sigma_{b,A}$. For NGRIP, we have increased its value from 0.8 to 0.9, and increased the minimum value from 0.15 to 0.2.

The formulation for the LIDIE standard deviation is:

$$\sigma_L(z) = \frac{\sigma_{b,L}}{\sigma_{b,A}} \cdot \frac{\sigma_A(z)}{1 + \frac{m_{A,loc}}{m_{A,loc}^{max}}} \tag{B4}$$

with $m_{A,loc}$ being the local mean accumulation rate and $m_{A,loc}^{max}$ its maximum value over the length of the core, $\sigma_{b,L}$ is a reference standard deviation. In this case, the variance on the LIDIE increases with the variance on the accumulation rate, i.e. with the deviation from present–day conditions. This is justified by the fact that we do not have a standardized way to link LIDIE to accumulation rate and/or temperature (firnification model or δ^{15}N based estimate). In section 3 we have reduced the value of the $\sigma_{b,L}$ coefficient from 0.6 to 0.3 as well as the minimum value possible (from 0.1 to 0.05) for NGRIP. This means that we have more confidence in our background LIDIE scenario than when building the AICC2012 chronology. The other coefficients have the same values as used to build AICC2012 (SOM Bazin et al., 2013).

Appendix C: GICC05 and MCE statistical assumptions

C1 Statistical assumptions to handle the annual layer counting variables

In the objective of better handling the MCE data, we make gaussian assumptions and reformulate the GICC05 layer counting with two probability density functions (pdf):

- The duration of an annual cycle identified as **certain** is normally distributed with a one year average and a zero standard deviation.
- The duration of an annual cycle identified as **uncertain** is normally distributed with a mean and a standard deviation set both to half a year.

The counting variables n_i and σ_i are statistical parameters of the gaussian distribution, which is to say the mean and standard deviation.

It must be noted that such formulation may be questioned: i) the annual layer counting as a discrete underlying nature and one might rather prefer to introduce discrete random variables to handle it, ii) the gaussian pdf applies to continuous random variables ranging from $-\infty$ to $+\infty$, which if far from being the case, iii) gaussian assumption based theorems are tricky to apply in the zero-variance limit assessed for annual layer identified as certain

C2 Sampling markers of age–difference and amount of error correlation accounted for: general case

Sampling markers of age–difference from the GICC05 layer counted chronology may lead to different amount of error correlation between individual measure of annual cycles. Let us first sample the markers on a T-time window and get the two constraints, $Y^T_{z_q,z_p}$ and $Y^T_{z_p,z_m}$, which measures the annual cycles in years in the two neighbouring depth intervals $[z_q, z_p]$ and $[z_p, z_m]$ along the core. The errors $\Sigma^T_{z_q,z_p}$ et $\Sigma^T_{z_p,z_m}$ associated with each marker writes:

$$\left(\Sigma^{T}_{z_q,z_p}\right)^2 = \sum_{i=q}^{p} {\sigma_i}^2 + 2\sum_{i=q}^{p}\sum_{j=q,j>i}^{p} \rho_{ij}\sigma_i\sigma_j \tag{C1}$$

$$\left(\Sigma^{T}_{z_p,z_m}\right)^2 = \sum_{i=p+1}^{m} {\sigma_i}^2 + 2\sum_{i=p+1}^{m}\sum_{j=p+1,j>i}^{m} \rho_{ij}\sigma_i\sigma_j \tag{C2}$$

$$\tag{C3}$$

If we double now the sampling rate, we get $2T$-time window markers with the single marker $Y^{2T}_{z_q,z_m}$, which measures the annual cycles in years over the depth interval $[z_q, z_m]$, instead of the two constraints $Y^{T}_{z_q,z_p}$ and $Y^{T}_{z_p,z_m}$.

$$Y^{2T}_{z_q,z_m} = Y^{T}_{z_q,z_p} + Y^{T}_{z_p,z_m} \tag{C4}$$

The error $\Sigma^{2T}_{z_q,z_m}$ associated with $2T$-time window marker $Y^{2T}_{z_q,z_m}$ now writes:

$$\left(\Sigma^{2T}_{z_q,z_m}\right)^2 = \sum_{i=q}^{m} {\sigma_i}^2 + 2\sum_{i=q}^{m}\sum_{j=q,j>i}^{m} \rho_{ij}\sigma_i\sigma_j \tag{C5}$$

Rearranging equation C5 in terms of the errors $\Sigma^{T}_{z_q,z_p}$ et $\Sigma^{T}_{z_p,z_m}$ gives:

$$\left(\Sigma^{2T}_{z_q,z_m}\right)^2 = \sum_{i=q}^{p} {\sigma_i}^2 + 2\sum_{i=q}^{p}\sum_{j=q,j>i}^{p} \rho_{ij}\sigma_i\sigma_j + \sum_{i=p+1}^{m} {\sigma_i}^2 + 2\sum_{i=p+1}^{m}\sum_{j=p+1,j>i}^{m} \rho_{ij}\sigma_i\sigma_j + 2\sum_{i=q}^{p}\sum_{j=p+1}^{m} \rho_{ij}\sigma_i\sigma_j = \left(\Sigma^{T}_{q,p}\right)^2 + \left(\Sigma^{T}_{p+1,m}\right)^2 + 2\sum_{i=q}^{p}\sum_{j=p+1}^{m} \rho_{ij}\sigma_i\sigma_j \quad \text{(C6)}$$

In equation C6, the red term corresponds to a part of the error accounted for in the $2T$-window marker $Y^{2T}_{z_q,z_m}$ that will never be accounted for in the case of the T-window markers $Y^{T}_{z_q,z_p}$ and $Y^{T}_{z_p,z_m}$. It corresponds to error correlations between annual layers i and j that are separated by the longest distance as they are located in the $[z_q, z_p]$ depth interval for the first layer, and in the next interval $[z_p, z_m]$ for the second. The longer range correlation can only be accounted for with the larger sampling rate. This point is illustrated with Figure 9.

It is worth it to note, that equation C6 simplifies further in only two cases regarding the ρ_{ij} correlation coefficients of the term highlighted in red:

- when the correlation coefficients are identically null, we get the sum of the squared errors:

$$\left(\Sigma^{2T}_{z_q,z_m}\right)^2 = \left(\Sigma^{T}_{q,p}\right)^2 + \left(\Sigma^{T}_{p+1,m}\right)^2 \quad \text{(C7)}$$

- when the correlation coefficient are identically set to 1, we get the squared sum of the errors:

$$\left(\Sigma^{2T}_{z_q,z_m}\right)^2 = \left(\Sigma^{T}_{q,p} + \Sigma^{T}_{p+1,m}\right)^2 \tag{C8}$$

Appendix D: The Datice data assimilation system

D1 Background and observation error covariance matrices

The background and observation errors $\tilde{\boldsymbol{\epsilon}}^b$ and $\boldsymbol{\epsilon}^o$ are measures of the background and observation distance to $\tilde{\boldsymbol{X}}^t$, which records the true but unknown model. In the Datice system $\tilde{\boldsymbol{X}}^t$ are the true correction functions to apply to accumulation, thinning and LIDIE (after exponential transformation). Errors $\tilde{\boldsymbol{\epsilon}}^b$ and $\boldsymbol{\epsilon}^o$ writes by definition:

$$\tilde{\boldsymbol{\epsilon}}^b = \tilde{\boldsymbol{X}}^b - \tilde{\boldsymbol{X}}^t \tag{D1}$$

$$\boldsymbol{\epsilon}^o = \boldsymbol{Y}^o - \mathbf{h}\left(\tilde{\boldsymbol{X}}^t\right) \tag{D2}$$

where vectors $\tilde{\boldsymbol{X}}^b$, $\boldsymbol{Y}^o$ store the background and observation data, and where $\mathbf{h}$ is the observation operator that maps the model space to the observation space. The background and observation error covariance matrices $\mathbf{B}$ and $\mathbf{R}$ matrices are defined as:

$$\mathbf{B} = \mathbf{E}\left[\tilde{\boldsymbol{\epsilon}}^b \tilde{\boldsymbol{\epsilon}}^{bT}\right] \tag{D3}$$

$$\mathbf{R} = \mathbf{E}\left[\boldsymbol{\epsilon}^o \boldsymbol{\epsilon}^{oT}\right] \tag{D4}$$

where $\mathbf{E}[\bullet]$ is the expected value operator, and ^{T} is the transpose operator.

D2 Analysed error covariance matrix

The analysed error $\tilde{\boldsymbol{\epsilon}}^a$ (random variable) is defined as follows:

$$\tilde{\boldsymbol{\epsilon}}^a = \tilde{\boldsymbol{X}}^a - \tilde{\boldsymbol{X}}^t \tag{D5}$$

where $\tilde{\boldsymbol{X}}^t$ records the true (but unknown) correction functions (i.e., the correction that would provide the exact true scenario of thinning, accumulation and LIDIE). The analysed error covariance matrix $\tilde{\mathbf{P}}^{\mathbf{a}}$ is given by:

$$\mathbf{P}^{\mathbf{a}} = \mathbf{E}\left[\tilde{\boldsymbol{\epsilon}}^a \tilde{\boldsymbol{\epsilon}}^{aT}\right] \tag{D6}$$

Appendix E: Analysed chronology and analysed errors

The ice age scale changes according to the correction function values $\tilde{\boldsymbol{X}} = (\tilde{\boldsymbol{\alpha}}(z), \tilde{\boldsymbol{\tau}}(z))^T$ as follows:

$$\Psi\left(\tilde{\boldsymbol{X}}\right) = \int_{z=0}^{z} \frac{\exp\left(-\tau(z')\right)\exp\left(-\alpha(z')\right)}{T^b(z')\,A^b(z')} D(z')\,dz' \tag{E1}$$

The optimized ice age is calculated by applying in equation E1 the optimized correction functions obtained after minimization of the cost function (equation 5):

$$\tilde{\boldsymbol{X}}^a = (\tilde{\boldsymbol{\alpha}}^a(z), \tilde{\boldsymbol{\tau}}^a(z), \tilde{\boldsymbol{\gamma}}^a(z))^T \tag{E2}$$

This gives the analysed chronology:

$$\Psi^a(z) = \Psi\left(\tilde{\boldsymbol{X}}^a\right) = \int_{z=0}^{z} \frac{\exp\left(-\tilde{\tau}^a(z')\right)\exp\left(-\tilde{\alpha}^a(z')\right)}{T^b(z')\,A^b(z')} D(z')\,dz' \tag{E3}$$

To approximate the *a posteriori* error of the analysed chronology, the covariances of errors of $\tilde{\boldsymbol{X}}^a$ are required. These covariances of errors are recorded in $\mathbf{P^a}$ the analysed error covariance matrix, which can be approximated:

$$\frac{1}{\mathbf{P^a}} \sim \frac{1}{\mathbf{B}} + \frac{1}{\mathbf{H^T R H}} \tag{E4}$$

where $\mathbf{B}$ and $\mathbf{R}$ are the background and observation error covariance matrices respectively D1, and where $\mathbf{H}$ is the tangent linear observation operator (linearization of $\boldsymbol{h}$ at $\tilde{\boldsymbol{X}}^a$.

Datice calculates the components of $\mathbf{P^a}$ at each depth level on the basis of equation E4. Importantly, $\mathbf{P^a}$ operates a balance between the background and observation errors. The $\mathbf{P^a}$ error covariance propagates to the analysed chronology $\Psi^a\left(\tilde{\boldsymbol{X}}^a\right)$. If we designate by E^a the *a posteriori* error of the analysed chronology, the corresponding analysed error covariance matrix $\mathbf{\Lambda}^a$ is by definition:

$$E^a = \Psi\left(\tilde{\boldsymbol{X}}^a\right) - \Psi\left(\tilde{\boldsymbol{X}}^t\right) \tag{E5}$$

$$\mathbf{\Lambda}^a = \mathbf{E}\left[E^a E^{aT}\right] \tag{E6}$$

Our purpose is to show how matrix $\mathbf{\Lambda}^a$ depends on matrix $\mathbf{P^a}$, then on the error matrices $\mathbf{B}$ and $\mathbf{R}$. We recall the steps to show this link, as first described in Lemieux-Dudon et al. (2009). One can first linearize the age scale of equation E1 around $\tilde{\boldsymbol{X}}^a$ (D5):

$$\Psi\left(\tilde{\boldsymbol{X}}^t\right) = \Psi\left(\tilde{\boldsymbol{X}}^a\right) - \tilde{\boldsymbol{\epsilon}}^{aT} \cdot \left[\left.\frac{\partial \Psi}{\partial \tilde{\boldsymbol{X}}}\right|_{\tilde{\boldsymbol{X}}^a}\right] + \circ\left(\|\tilde{\boldsymbol{\epsilon}}^a\|\right) \tag{E7}$$

Inserting equation E7 in equation E5 enables one to approximate the *a posteriori* error E^a:

$$E^a \sim \tilde{\boldsymbol{\epsilon}}^{aT} \cdot \left[\left.\frac{\partial \Psi}{\partial \tilde{\boldsymbol{X}}}\right|_{\tilde{\boldsymbol{X}}^a}\right] \tag{E8}$$

Importantly, the later approximation is valid if $\tilde{\boldsymbol{\epsilon}}^a$ are sufficiently small perturbations, i.e., the correction functions $\tilde{\boldsymbol{X}}^a$ must be close to the true scenario $\tilde{\boldsymbol{X}}^t$. Under this strong assumption, equation E8 leads to:

$$E^a E^{aT} \sim \left[\frac{\partial \Psi}{\partial \tilde{\boldsymbol{X}}} \bigg|_{\tilde{\boldsymbol{X}}^a} \right]^T \tilde{\boldsymbol{\epsilon}}^a \tilde{\boldsymbol{\epsilon}}^{aT} \left[\frac{\partial \Psi}{\partial \tilde{\boldsymbol{X}}} \bigg|_{\tilde{\boldsymbol{X}}^a} \right] \tag{E9}$$

And finally, from equation E9, one can approximate the error matrix of the ice age $\boldsymbol{\Lambda}^a$ by applying the expected value operator to equations E9 and by using equation D6:

$$\boldsymbol{\Lambda}^a = \sim \left[\frac{\partial \Psi}{\partial \tilde{\boldsymbol{X}}} \bigg|_{\tilde{\boldsymbol{X}}^a} \right]^T \mathbf{P}^a \left[\frac{\partial \Psi}{\partial \tilde{\boldsymbol{X}}} \bigg|_{\tilde{\boldsymbol{X}}^a} \right] \tag{E10}$$

Datice applies equation E10 to approximate the covariances of errors of the analysed chronology. This approximation especially requires that the optimum correction functions $\tilde{\boldsymbol{X}}^a$ obtained after minimization of the cost function remain sufficiently close to the true scenario $\tilde{\boldsymbol{X}}^t$. On the assumption of normally distributed errors, matrix $\boldsymbol{\Lambda}^a$ provides the standard deviation of the analysed age scale. The process to calculate the analysed error of the gas age scale is similar but relies on equation (A2).

E1 Balance between background and observation error and impact on the analysis

The variances of errors of the analysed chronology cumulate the error covariances recorded in matrix $\mathbf{P^a}$ (equation E10). The age solution and its error are therefore largely determined by the balance between observation and background errors (equation E4). To fix ideas, instead of matrices $\mathbf{P}^a$, $\mathbf{R}$ and $\mathbf{B}$, let us suppose we deal with the scalars σ^a, σ^o and σ^b. With such simplification, equation E4 writes:

$$\frac{1}{{\sigma_a}^2} = \frac{1}{{\sigma_b}^2} + \frac{1}{{\sigma_o}^2} \tag{E11}$$

According to the ratio bewteen observation and background errors, there are two extreme configurations:

- if $\sigma_o \ll \sigma_b$, the minimization and the solution are strongly constrained by the observation and the analysed error tends to be the observation error:

$$\sigma_a \sim \sigma_o \tag{E12}$$

- to the opposite, if $\sigma_b \ll \sigma_o$, the background scenario dominates and the solution resembles the background. The analysed error tends to the background error:

$$\sigma_a \sim \sigma_b \tag{E13}$$

Intermediate background to observation error ratio leads to intermediate analysed solution and error. In the special case of equal amount of errors in observation and background, i.e., $\sigma = \sigma_o \sim \sigma_b$ the analysed error writes:

$$\sigma_a \sim \frac{\sigma}{\sqrt{2}} \tag{E14}$$

Acknowledgements. We thank Eric Wolff for his comments on a preliminary version of this article. This project was funded by the "Fondation de France Ars Cuttoli". This work was supported by Labex L-IPSL which is funded by the ANR (Grant n°ANR-10-LABX-0018). This is LSCE contribution no XX.

References

Andersen, K. K., Svensson, A., Johnsen, S. J., Rasmussen, S. O., Bigler, M., Röthlisberger, R., Ruth, U., Siggaard-Andersen, M.-L., Peder Steffensen, J., Dahl-Jensen, D., Vinther, B. M., and Clausen, H. B.: The Greenland Ice Core Chronology 2005, 15 42 ka. Part 1: constructing the time scale, Quaternary Science Reviews, 25, 3246–3257, doi:10.1016/j.quascirev.2006.08.002, 2006.

Austin, W., Hibbert, F., Rasmussen, S., Peters, C., Abbott, P., and Bryant, C.: The synchronization of palaeoclimatic events in the North Atlantic region during Greenland Stadial 3 (ca 27.5 to 23.3 kyr b2k), Quaternary Science Reviews, 36, 154–163, doi:10.1016/j.quascirev.2010.12.014, 2012.

Austin, W. E. and Hibbert, F. D.: Tracing time in the ocean: a brief review of chronological constraints (60–8 kyr) on North Atlantic marine event-based stratigraphies, Quaternary Science Reviews, 36, 28–37, doi:10.1016/j.quascirev.2012.01.015, 2012.

Bazin, L., Landais, A., Lemieux-Dudon, B., Toyé Mahamadou Kele, H., Veres, D., Parrenin, F., Martinerie, P., Ritz, C., Capron, E., Lipenkov, V., Loutre, M.-F., Raynaud, D., Vinther, B., Svensson, A., Rasmussen, S., Severi, M., Blunier, T., Leuenberger, M., Fischer, H., Masson-Delmotte, V., Chappellaz, J., and Wolff, E.: An optimized multi-proxies, multi-site Antarctic ice and gas orbital chronology (AICC2012): 120-800 ka, Climate of the Past, 9, 1715–1731, doi:10.5194/cp-9-1715-2013, 2013.

Blockley, S., Lane, C., Turney, C., and Bronk Ramsey, C.: The INTegration of Ice core, MArine and TErrestrial records of the last termination (INTIMATE)60,000 to 8000 BP, Quaternary Science Reviews, 36, 1–, doi:10.1016/j.quascirev.2011.10.001, 2012a.

Blockley, S. P., Lane, C. S., Hardiman, M., Rasmussen, S. O., Seierstad, I. K., Steffensen, J. P., Svensson, A., Lotter, A. F., Turney, C. S., and Bronk Ramsey, C.: Synchronisation of palaeoenvironmental records over the last 60,000 years, and an extended INTIMATE event stratigraphy to 48,000 b2k, Quaternary Science Reviews, 36, 2–10, doi:10.1016/j.quascirev.2011.09.017, 2012b.

Buiron, D., Chappellaz, J., Stenni, B., Frezzotti, M., Baumgartner, M., Capron, E., Landais, A., Lemieux-Dudon, B., Masson-Delmotte, V., Montagnat, M., Parrenin, F., and Schilt, A.: TALDICE-1 age scale of the Talos Dome deep ice core, East Antarctica, Climate of the Past, 7, 1–16, doi:10.5194/cp-7-1-2011, 2011.

Capron, E., Landais, A., Buiron, D., Cauquoin, A., Chappellaz, J., Debret, M., Jouzel, J., Leuenberger, M., Martinerie, P., Masson-Delmotte, V., Mulvaney, R., Parrenin, F., and Prié, F.: Glacial-interglacial dynamics of Antarctic firns: comparison between simulations and ice core air-d15N measurements, Climate of the Past, 9, 983–999, doi:10.5194/cp-9-983-2013, 2013.

Cutler, N. N., Raymond, C. F., Waddington, E. D., Meese, D. A., and Alley, R. B.: The effect of ice-sheet thickness change on the accumulation history inferred from GISP2 layer thicknesses, Annals of Glaciology, 21, 26–32, 1995.

Dansgaard, W. and Johnsen, S. J.: A flow model and a time scale for the ice core from Camp Century, Greenland, Journal of Glaciology, 8, 215–223, 1969.

Davies, S. M., Abbott, P. M., Pearce, N. J., Wastegard, S., and Blockley, S. P.: Integrating the INTIMATE records using tephrochronology: rising to the challenge, Quaternary Science Reviews, 36, 11–27, doi:10.1016/j.quascirev.2011.04.005, 2012.

Desroziers, G., Berre, L., Chabot, V., and Chapnik, B.: A posteriori diagnostics in an ensemble of perturbed analyses, Monthly Weather Review, 137, 3420–3436, 2009.

EPICA Community Members: One-to-one coupling of glacial climate variability in Greenland and Antarctica, Nature, 444, 195–198, doi:10.1038/nature05301, 2006.

EPICA Community Members: Stable oxygen isotopes of ice core EDML, PANGAEA, doi:10.1594/PANGAEA.754444, 2010.

Goujon, C., Barnola, J.-M., and Ritz, C.: Modeling the densification of polar firn including heat diffusion: Application to close-off characteristics and gas isotopic fractionation for Antarctica and Greenland sites, Journal of Geophysical Research (Atmospheres), 108, 4792, doi:10.1029/2002JD003319, 2003.

Guillevic, M., Bazin, L., Landais, A., Masson- Delmotte, V., Blunier, T., Buchardt, S. L., Capron, E., Kindler, P., Leuenberger, M., Minster, B., Orsi, A., Prie, F., and Vinther, B. M.: Spatial gradients of temperature, accumulation and $\delta^{18}O$-ice in Greenland over a series of Dansgaard-Oeschger events, Climate of the Past, 9, 1029–1051, doi:10.5194/cp-9-1029-2013, 2013.

Huber, C., Beyerle, U., Leuenberger, M., Schwander, J., Kipfer, R., Spahni, R., Severinghaus, J. P., and Weiler, K.: Evidence for molecular size dependent gas fractionation in firn air derived from noble gases, oxygen, and nitrogen measurements, Earth and Planetary Science Letters, 243, 61–73, doi:10.1016/j.epsl.2005.12.036, 2006.

Johnsen, S. J., Dahl-Jensen, D., Gundestrup, N., Steffensen, J. P., Clausen, H. B., Miller, H., Masson-Delmotte, V., Sveinbjornsdottir, A. E., and White, J.: Oxygen isotope and palaeotemperature records from six Greenland ice-core stations: Camp Century, Dye-3, GRIP, GISP2, Renland and NorthGRIP, Journal of Quaternary Science, 16, 299–307, doi:10.1002/jqs.622, 2001.

Jouzel, J., Masson-Delmotte, V., Cattani, O., Dreyfus, G., Falourd, S., Hoffmann, G., Minster, B., Nouet, J., Barnola, J. M., Chappellaz, J., Fischer, H., Gallet, J. C., Johnsen, S., Leuenberger, M., Loulergue, L., Luethi, D., Oerter, H., Parrenin, F., Raisbeck, G., Raynaud, D., Schilt, A., Schwander, J., Selmo, E., Souchez, R., Spahni, R., Stauffer, B., Steffensen, J. P., Stenni, B., Stocker, T. F., Tison, J. L., Werner, M., and Wolff, E. W.: Orbital and Millennial Antarctic Climate Variability over the Past 800,000 Years, Science, 317, 793–, doi:10.1126/science.1141038, 2007.

Kindler, P., Guillevic, M., Baumgartner, M., Schwander, J., Landais, A., Leuenberger, M., Spahni, R., Capron, E., and Chappellaz, J.: Temperature reconstruction from 10 to 120 kyr b2k from the NGRIP ice core, Climate of the Past, 10, 887–902, doi:10.5194/cp-10-887-2014, 2014.

Landais, A., Waelbroeck, C., and Masson-Delmotte, V.: On the limits of Antarctic and marine climate records synchronization: Lag estimates during marine isotopic stages 5d and 5c, Paleoceanography, 21, PA1001, doi:10.1029/2005PA001171, 2006.

Lemieux-Dudon, B., Parrenin, F., and Blayo, E.: A probabilistic method to construct a common and optimal chronology for an ice core, Physics of Ice Core Records, 2009.

Lemieux-Dudon, B., Blayo, E., Petit, J.-R., Waelbroeck, C., Svensson, A., Ritz, C., Barnola, J.-M., Narcisi, B. M., and Parrenin, F.: Consistent dating for Antarctic and Greenland ice cores, Quaternary Science Reviews, 29, 8–20, doi:10.1016/j.quascirev.2009.11.010, 2010.

Lorius, C., Ritz, C., Jouzel, J., Merlivat, L., and Barkov, N. I.: A 150,000-year climatic record from Antarctic ice, Nature, 316, 591–596, doi:10.1038/316591a0, 1985.

Members, W. D. P.: Onset of deglacial warming in West Antarctica driven by local orbital forcing, Nature, 500, 440–444, http://dx.doi.org/10.1038/nature12376, 2013.

NorthGRIP Community Members: High-resolution record of Northern Hemisphere climate extending into the last interglacial period, Nature, 431, 147–151, doi:10.1038/nature02805, 2004.

Parrenin, F., Rémy, F., Ritz, C., Siegert, M. J., and Jouzel, J.: New modeling of the Vostok ice flow line and implication for the glaciological chronology of the Vostok ice core, Journal of Geophysical Research (Atmospheres), 109, D20102, doi:10.1029/2004JD004561, 2004.

Parrenin, F., Dreyfus, G., Durand, G., Fujita, S., Gagliardini, O., Gillet, F., Jouzel, J., Kawamura, K., Lhomme, N., Masson-Delmotte, V., Ritz, C., Schwander, J., Shoji, H., Uemura, R., Watanabe, O., and Yoshida, N.: 1-D-ice flow modelling at EPICA Dome C and Dome Fuji, East Antarctica, Climate of the Past, 3, 243–259, doi:10.5194/cp-3-243-2007, 2007.

Petit, J. R., Jouzel, J., Raynaud, D., Barkov, N. I., Barnola, J.-M., Basile, I., Bender, M., Chappellaz, J., Davis, M., Delaygue, G., Delmotte, M., Kotlyakov, V. M., Legrand, M., Lipenkov, V. Y., Lorius, C., Pépin, L., Ritz, C., Saltzman, E., and Stievenard, M.: Climate and atmospheric history of the past 420,000 years from the Vostok ice core, Antarctica, Nature, 399, 429–436, doi:10.1038/20859, 1999.

Rasmussen, S. O., Andersen, K. K., Svensson, A. M., Steffensen, J. P., Vinther, B. M., Clausen, H. B., Siggaard-Andersen, M.-L., Johnsen, S. J., Larsen, L. B., Dahl-Jensen, D., Bigler, M., Röthlisberger, R., Fischer, H., Goto-Azuma, K., Hansson, M. E., and Ruth, U.: A new Greenland ice core chronology for the last glacial termination, Journal of Geophysical Research (Atmospheres), 111, D06102, doi:10.1029/2005JD006079, 2006.

Stenni, B., Buiron, D., Frezzotti, M., Albani, S., Barbante, C., Bard, E., Barnola, J. M., Baroni, M., Baumgartner, M., Bonazza, M., Capron, E., Castellano, E., Chappellaz, J., Delmonte, B., Falourd, S., Genoni, L., Iacumin, P., Jouzel, J., Kipfstuhl, S., Landais, A., Lemieux-Dudon, B., Maggi, V.,

Masson-Delmotte, V., Mazzola, C., Minster, B., Montagnat, M., Mulvaney, R., Narcisi, B., Oerter, H., Parrenin, F., Petit, J. R., Ritz, C., Scarchilli, C., Schilt, A., Schüpbach, S., Schwander, J., Selmo, E., Severi, M., Stocker, T. F., and Udisti, R.: Expression of the bipolar see-saw in Antarctic climate records during the last deglaciation, Nature Geoscience, 4, 46–49, doi:10.1038/ngeo1026, 2011.

Svensson, A., Andersen, K. K., Bigler, M., Clausen, H. B., Dahl-Jensen, D., Davies, S. M., Johnsen, S. J., Muscheler, R., Parrenin, F., Rasmussen, S. O., Röthlisberger, R., Seierstad, I., Steffensen, J. P., and Vinther, B. M.: A 60 000 year Greenland stratigraphic ice core chronology, Climate of the Past, 4, 47–57, doi:10.5194/cp-4-47-2008, 2008.

Tarantola, A.: Inverse Problem Theory and Methods for Model Parameter Estimation, Society for Industrial and Applied Mathematics, doi:10.1137/1.9780898717921, 2005.

Veres, D., Bazin, L., Landais, A., Toye Mahamadou Kele, H., Lemieux-Dudon, B., Parrenin, F., Martinerie, P., Blayo, E., Blunier, T., Capron, E., Chappellaz, J., Rasmussen, S., Severi, M., Svensson, A., Vinther, B., and Wolff, E.: The Antarctic ice core chronology (AICC2012): an optimized multi-parameter and multi-site dating approach for the last 120 thousand years, Climate of the Past, 9, 1733–1748, doi:10.5194/cp-9-1733-2013, 2013.

Vinther, B. M., Clausen, H. B., Johnsen, S. J., Rasmussen, S. O., Andersen, K. K., Buchardt, S. L., Dahl-Jensen, D., Seierstad, I. K., Siggaard-Andersen, M.-L., Steffensen, J. P., Svensson, A., Olsen, J., and Heinemeier, J.: A synchronized dating of three Greenland ice cores throughout the Holocene, Journal of Geophysical Research (Atmospheres), 111, D13102, doi:10.1029/2005JD006921, 2006.

Walker, M., Lowe, J., Blockley, S. P., Bryant, C., Coombes, P., Davies, S., Hardiman, M., Turney, C. S., and Watson, J.: Late glacial and early Holocene palaeoenvironmental 'events' in Sluggan Bog, Northern Ireland: comparisons with the Greenland NGRIP GICC05 event stratigraphy, Quaternary Science Reviews, 36, 124–138, doi:10.1016/j.quascirev.2011.09.008, 2012.

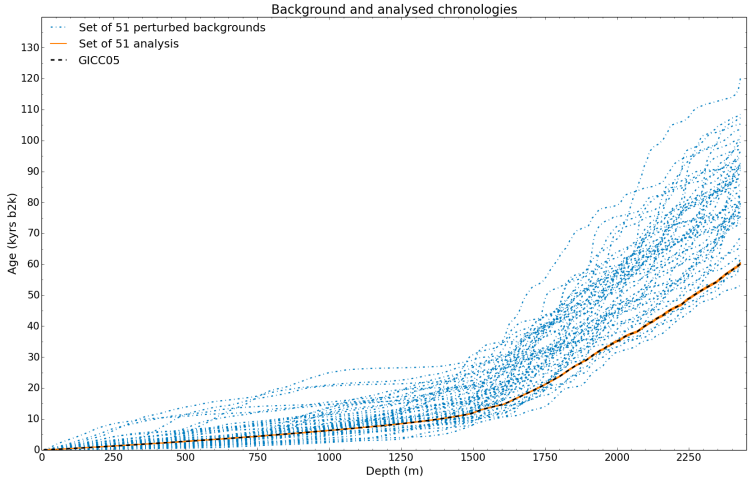

Figure 1. Twin experiments: background (dashed blue lines) and analysed (orange lines) chronologies of the 51 twim experiments. The GICC05 chronology is represented by the dashed black line for comparison.

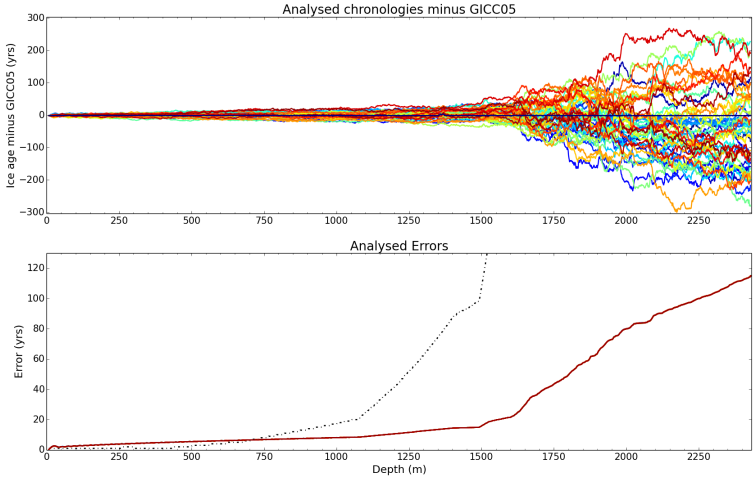

Figure 2. Analysed chronologies of the 51 twin experiments. Top: Comparison of the analysed chronologies with GICC05. Bottom: analysed errors of the 51 twin experiments (red). The dashed black line represents the Maximum Counting Error associated with GICC05 and considered in GICC05 as equivalent to a 2–sigma uncertainty.

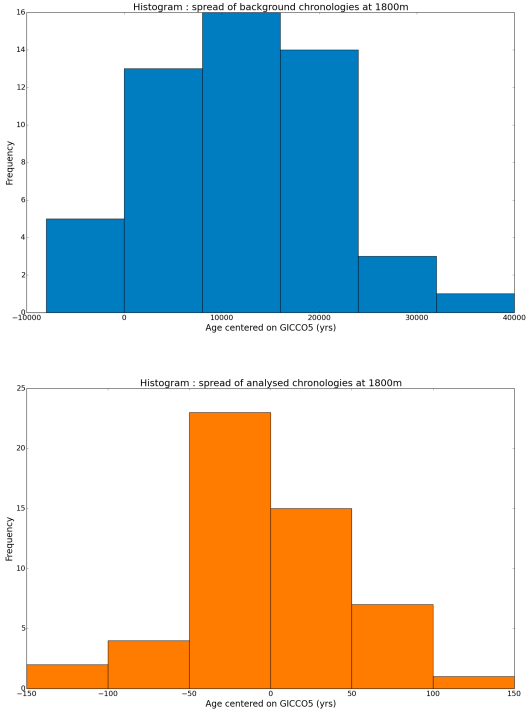

Figure 3. Histograms of the 51 twin experiments for the background (blue) and analysed (red) chronologies at depth 1800 m for NGRIP ice core.

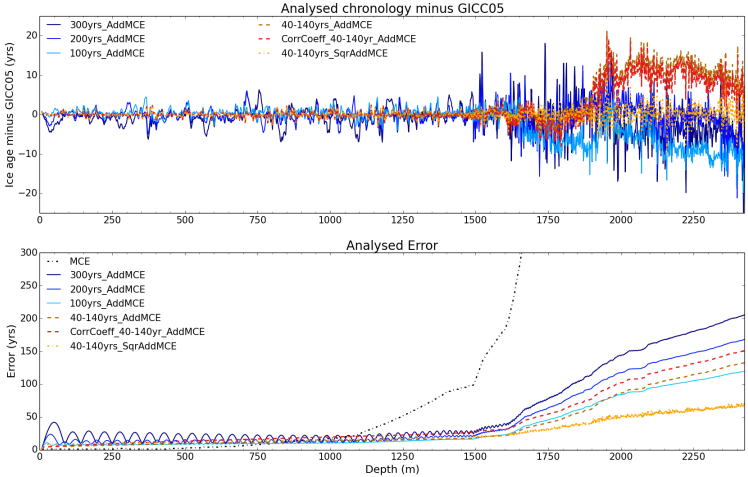

Figure 4. Sensitivity of the age and error solution to the age–difference markers sampling and to the MCE error assumptions. The difference between analysed chronologies and GICC05 age scale are shown on the top panel. Analysed errors and MCE are plotted on the bottom panel. The simulations settings are: (i) three different uniform sampling rates (300, 200 and 100 years) and (ii) one adaptive sampling rate ranging from 40 to 140 years. The markers errors are derived under the **AddMCE** assumption (full correlation between annual cycles), except for the 40-140yrs_SqrAddMCE simulation that is ran under the **SqrAddMCE** assumption (correlation cut-off above 20 years).

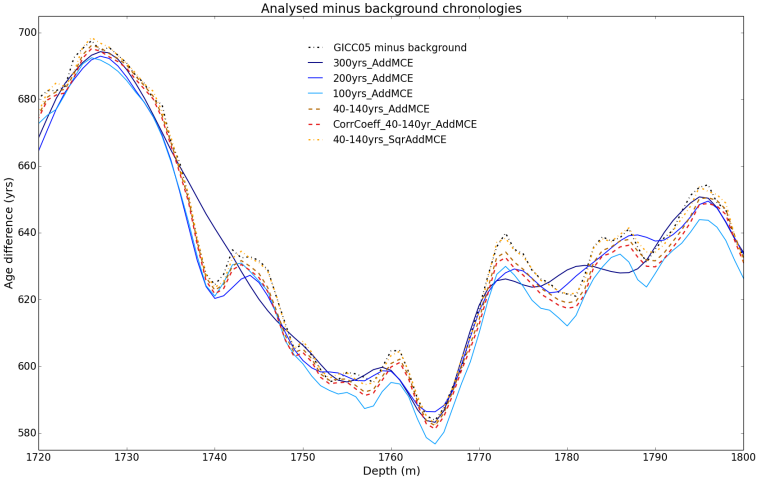

Figure 5. Sensitivity of the age solution to the age–difference markers sampling. The simulations settings are: (i) three different uniform sampling rates (plain blue lines: 300, 200 and 100 years) and (ii) one adaptive rate ranging from 40 to 140 years (dashed colored lines). The markers errors are derived under the **AddMCE** assumption (full correlation between annual cycles), except the 40-140yrs_SqrAddMCE simulation that is ran under the **SqrAddMCE** assumption (correlation cut-off above 20 years). The curves represent the difference between the different analysed and background chronologies. The difference GICC05–background is displayed for comparison (dashed black line).

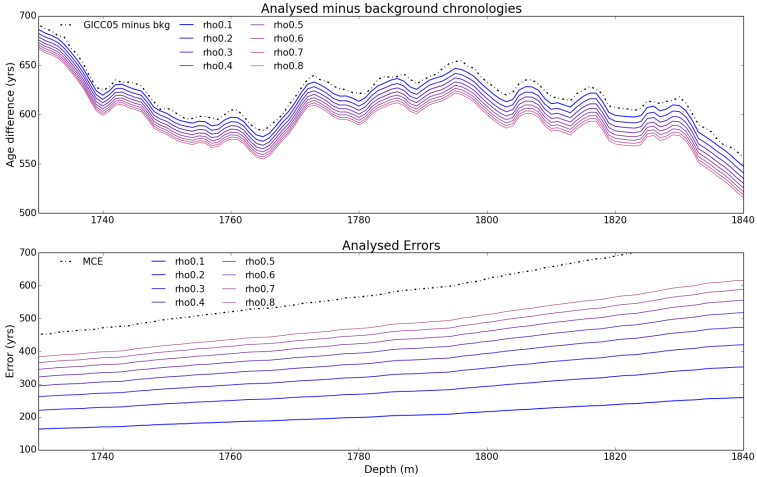

Figure 6. Sensitivity of the solution to correlation coefficient values applied between markers of age–difference (Infinite depths range case). Top panel: GICC05 minus background chronology (black dashed line), Difference between analysed and background chronologies (blue to pink lines). Bottom panel: MCE error (black dashed line), analysed errors (blue to pink lines) The markers of age–difference are sampled every 100 years on GICC05, and correlation coefficients range from 0.8 to 0.2. The MCE error assumption is **AddMCE** (full error correlation between cycles).

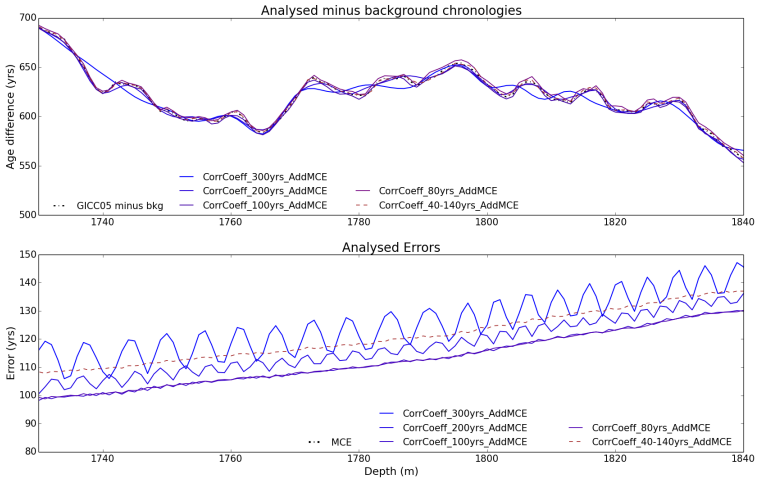

Figure 7. Sensitivity of the solution to correlation coefficient values applied between markers of age–difference (Finite depths range case). Top panel: GICC05 minus background chronology (black dashed line) and difference between analysed and background chronologies. Bottom panel: MCE error (black dashed line), analysed errors (blue to pink lines) The markers of age–difference are correlated through a correlation function (gaussian times triangle), the correlation length is 300 years. Uniform marker sampling at 80, 100, 200 and 300 years rates are shown with the blue to pink lines. The adaptive sampling rate (40-140yrs) is shown in brown. The MCE error assumption is **AddMCE** (full error correlation between cycles).

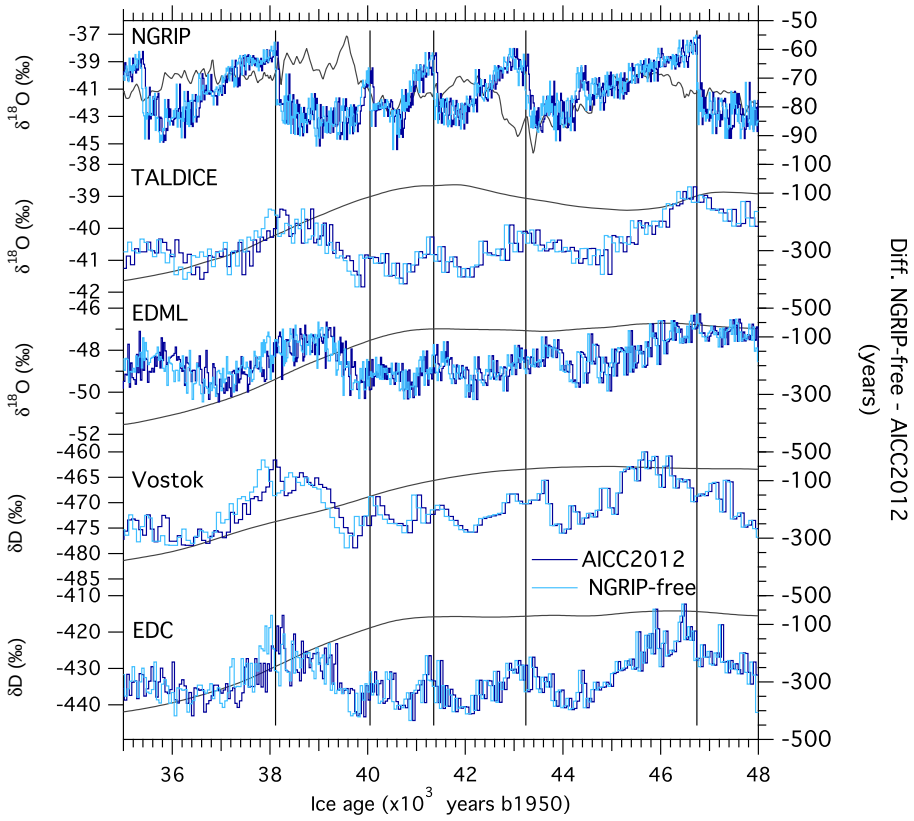

Figure 8. Comparison of NGRIP δ^{18}O (NorthGRIP Community Members, 2004), TALDICE δ^{18}O (Stenni et al., 2011), EDML δ^{18}O (EPICA Community Members, 2006, 2010), Vostok δD (Petit et al., 1999) and EDC δD (Jouzel et al., 2007) water isotopes on different coherent chronologies (AICC2012 in dark blue and NGRIP-free in light blue). The differences between the NGRIP-free and AICC2012 chronologies for each sites are represented by the black lines.

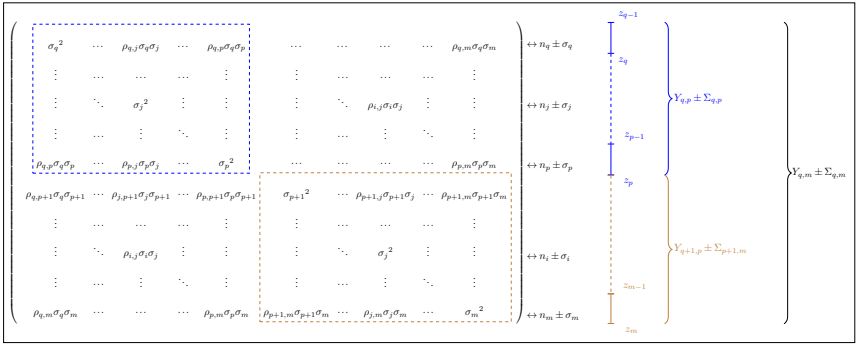

Figure 9. The error covariance matrix $\mathbf{R}$ associated with a measure of duration $Y^{2T}_{z_q,z_m}$ sampled at a $2T$ years rate on a layer counted chronology, e.g GICC05. The matrix stores error information related to the measures of annual cycles on the depths interval $[z_q, z_m]$. The diagonal elements record the error variances ${\sigma_i}^2$ associated with each identified annual cycle, while the non–diagonal elements store the error covariances, with especially the error correlation coefficient ρ_{ij} between pairs of annual layers i et j. The error $\Sigma^{2T}_{z_q,z_m}$ associated with marker $Y^{2T}_{z_q,z_m}$ takes into account the whole error correlations stored in the $\mathbf{R}$ matrix. If the measures of duration are rather sampled at the T sampling rate (i.e., half the previous rate), the marker of age–difference $Y^{2T}_{z_q,z_m}$ splits into two markers: (i) $Y^{T}_{z_q,z_p}$ (in blue) and (ii) $Y^{T}_{z_p,z_m}$ (in brown). The error $\Sigma^{T}_{z_q,z_p}$ associated with $Y^{T}_{z_q,z_p}$ will only account for the correlation of the upper diagonal block of $\mathbf{R}$ (dashed blue line around block). Symmetrically, the error $\Sigma^{T}_{z_p,z_m}$ associated with $Y^{T}_{z_p,z_m}$ will only account for the correlation of the lower diagonal blocks of $\mathbf{R}$ (dashed brown line around block). Error correlations of the non-diagonal blocks of $\mathbf{R}$ between annual layers $i \in [z_q, z_p]$ and $j \in [z_p, z_m]$ are only accounted for in the total error with the $2T$ sampling rate.

Table 1. Summary of the simulation configurations

Name	MCE error assumption	Sampling	Correlation coefficient
300yrs_AddMCE	AddMCE	300yrs	None
200yrs_AddMCE	AddMCE	200yrs	None
100yrs_AddMCE	AddMCE	100yrs	None
40-140yrs_AddMCE	AddMCE	Adaptative	None
40-140yrs_SqrAddMCE	SqrAddMCE	Adaptative	None
CorrCoeff_40-140yrs_AddMCE	AddMCE	Adaptative	L^{ad} =300yrs

Table 2. New Δdepth markers of NGRIP deduced from the data of Kindler et al. (2014)

depth (m)	Δdepth (m)	σ (m)	Event
1490.2	25.07	2.5	Holocene
1520.5	21.84	2.5	
1574.4	23.51	2.5	
1603.0	26.42	2.5	D-O 1
1792.7	25.07	2.5	D-O 2
1868.1	22.62	2.5	D-O 3
1888.4	21.87	2.5	D-O 4
1950.6	21.32	2	D-O 5
1972.6	20.42	2	D-O 6
2007.8	19.22	2	D-O 7
2099.9	17.77	2	D-O 8

Table 3. Summary of the simulation configurations

Experiment	Variance profile	A^b	T^b	C^b	Objective
Twin experiments (2.2)	Changing with depth Bazin et al. (2013)	-	σ_b of thinning divided by 3	-	Avoid correction on the thinning in experiment with ice age only
Sensitivity to sampling and MCE (2.4.1)	Constant with depth	$\sigma_b = 0.8$ triangular ρ_b function 2500yrs width	$\sigma_b = 0.5$ triangular ρ_b function 60m width	-	Simplify the experiment
Correlation between markers (2.4.2)	Constant with depth	$\sigma_b = 3.2$ triangular ρ_b function 2500yrs width	$\sigma_b = 2$ triangular ρ_b function 60m width	-	Reinforce the marker constraints : $\sigma_b \gg \sigma_o$